Impact of a localized solid cylinder on entropy generation and mixed convection of nanofluids in a lid-driven trapezoidal cavity

Muhamad S. Ishak^{a,b}, Ammar I. Alsabery^a, Ishak Hashim^{a,*} and A.J. Chamkha^{c,d}

^{a}Department of Mathematical Sciences, Faculty of Science & Technology, Universiti Kebangsaan Malaysia, 43600 UKM Bangi, Selangor, Malaysia

^{b}Department of Engineering, College of Foundation and Diploma Studies, Universiti Tenaga Nasional, 43000, Kajang, Selangor, Malaysia

^{c}Faculty of Engineering, Kuwait College of Science and Technology, Doha District 35001, Kuwait

^{d}Center of Excellence in Desalination Technology, King Abdulaziz University, P.O. Box 80200, Jeddah 21589, Saudi Arabia

November 6, 2020

Abstract

The problem of entropy generation and mixed convection in a nanofluid trapezoidal cavity with an internal solid cylinder is studied numerically using the finite difference method. The bottom wall is thermally insulated while the upper wall slides with uniform velocity from left to right and cooled isothermally. Remainder of these walls are kept adiabatic. Water-based nanofluids with Al_2O_3 nanoparticles are chosen for the investigation. The Boussinesq approximation is applicable. The influence of Reynolds number, Richardson number, dimensionless radius of the solid cylinder, location of the solid cylinder and nanoparticles of volume fraction on streamlines, isotherms, isentropic as well as the local and average Nusselt number were investigated. It was found that the location and size of the solid cylinder are important control parameters for optimizing heat transfer and Bejan number within the partially heated trapezoid cavity.

Keywords: Entropy generation; Mixed convection flow; Trapezoidal cavity; Nanofluid, Circular solid cylinder; Finite element method

1 Introduction

Mixed convective heat transfer in enclosures is very important in various engineering application such as solar panels, materialcs processor, solar ponds, heat exchangers and

---

*Corresponding author: ishak_h@ukm.edu.my

many more. The combination of shear effect and buoyancy force have been investigated by many researchers. Mixed convection in square or rectangles cavities have been investigated in Roy et al. [1], Abbasian Arani et al. [2], Khorasanizadeh et al. [3], Sebdani et al. [4], ,Nayak et al. [5] and Sivasankaran et al. [6]. Some researchers have investigated numerical studies on mixed convection in trapezoidal cavities. Arefmanesh et al. [7] concluded that the effective thermal conductivity of nanofluid leads in heat transfer and entropy generation inside the enclosure for a variable property model. Non isothermal bottom wall plays a pre-eminent role to multiple steady states in either natural convection dominated regime or mixed convection regime in convection dominated heat transport regime have been found by Bhattacharya et al. [8]. Tmartnhad et al. [9] investigated mixed convection in two-dimensional trapezoidal cavity with two openings and heated from below. They concluded that heat transfer and flow structure pivot on the inlet opening site. Similar with Tmartnhad, Kareem et al. [10] also investigated mixed convection in trapezoidal cavity but different types of nanofluid and no inlet opening site. The outcome shows that a wide range of nanofluids have higher Nusselt number compared with pure water. They also found that the Nusselt number increments as the volume fraction increases and the rotational angle decline yet diminishes as the measurement of the nanopacrticles of nanofluid increases. Selimefendigil and ztop [11] investigated mixed convection in a lid driven trapezoidal cavity filled with alumina-water nanofluid effect of an inclined magnetic field for three different electrical conductivity models. The result reveals that the value of Richardson number, strength of the magnetic field and solid particle volume fractions enhance and disparity between the average Nusselt number increases for system with various electrical conductivity models.Aghaei et al. [12] investigated the effects of magnetic field ina a trapezoidal enclosure on the flow field, heat transfer and entropy generation of Cu water nanofluid mixed convection. The top lid is cold and moves to the right or left, the bottom wall is warmer, and the side walls are separated from the horizon at various angles. They discovered that the convection of nanofluid and strength of flow decrease while the flow tends toward numbers natural convection and finally towards pure conduction by introducing and enhancing the magnetic field while entropy generation due to friction is negligible and the total entropy generation is mainly due to irreversibility associated with heat transfer. Abdullah A. A. A. Al-Rashed [13] investigated the flow field and heat transfer of a water-copper nanofluid with variable properties in a trapezoidal enclosure saturated with porous media. They discovered that with increasing Reynolds number for all Darcy numbers, aspect ratios and volume fraction of nanoparticles, the average Nusselt number increases. The effect of the tilt angle of the cavity on the mixed convection heat transfer inside two separate lid-driven trapezoidal cavities was investigated by Hasib et al. [14]. One heated the wall on short base and the other heated the wall on a long base. They discovered that the heat transfer and flow characteristics inside the cavities depend strongly on Reynold and Grashof numbers. Chamkha and Ismael [15] examined the mixed convection within a Cu-water nanofluid filled trapezoidal by the action of lid-driving of the right hot inclined side wall under the effect of a constant magnetic field. They found that, depending on the direction of the lid, the action of the Nusselt number varies from the Richardson number. The numerical results for heat transfer through mixed convection in an incompressible steady lid driven fluid flow inside a trapezoidal cavity in the presence of a uniform magnetic field were investigated by T. Javed [16]. The findings show that for Ra = 100,000, the effects of moving lid become negligible, although increasing Rayleigh number leads to greater streamline circulation and convection dominant effects within the enclosure. Mamun et al. [17] conducted a research on the mixed convection heat transfers in a two dimensional trapezoidal cavity with constant heat flux at the heated bottom wall while the isothermal moving top wall in the horizontal direction numerically. They discovered

that the heat transfer rate is influenced by the rotational angle of the trapezoidal cavity and the direction of the lid motion. Ababaei et al. [18] conducted the entropy generation of double diffusive mixed convection inside a right angled trapezoidal cavity with a partially heated and salted bottom wall. The result shows the average Nusselt number decreases as the Lewis number increases, while the total entropy generation increases.

Researchers have been conducting the research with either base fluid or nanofluid or both. Gibanov et al. [19] conducted conjugate mixed convection and entropy generation of alumina-water nanofluid in a lid driven cavity with a bottom solid wall. The outcome shows that bottom wall thickness and volume fraction of nanoparticles plays an important role in enhancing heat transfer. Astanina et al. [20] studied the mixed convection of alumina-water nanofluid in a lid driven cavity with two porous layers with different thermal properties, permeability and porosity located on the bottom wall. They discovered that addition of nanoparticles contributes to the enhancement of heat transfer in natural convection while an increase in the volume fraction of nanoparticles leads to a reduction in heat transfer for mixed and forced convection. Abu-Nada and Chamkha [21] investigated the mixed convection flow in a lid driven inclined square enclosure filled with alumina-water nanofluid. They found that due to the existence of nanoparticles, significant heat transfer enhancement can be achieved. Mehmood et al. [22] examined the mixed convection in alumina-water nanoluid filled lid driven square cavity filled with an isothermally heated square blockage with magnetic filed effect. They found that as nanoparticle volume fraction increases, the average Nusselt number and kinetic energy increase. The findings also show that with a rise in the magnetic field, average Nusselt number, average entropy generation due to heat transfer, Bejan number, and kinetic energy decrease. Goodarzi et al. [23] investigated the laminar and turbulent mixed convection heat transfer of water-Cu nanofluids in a rectangular shallow cavity utilizing a two phase mixture model. Increasing the volume fraction of nanoparticles is shown to increase the coefficient of convective heat transfer and thus the Nusselt number for specific Grashof and Richardson number. The laminar mixed convection flow in single and double lid square cavities filled with an alumina water nanofluid was investigated numerically by Chamkha and Abu-Nada [24]. Due to the existence of nanoparticles, it is observed that significant heat transfer enhancement can be accomplished and that this is accentuated by increasing the nanoparticles volume fraction at moderate and high Richardson number using both nanofluid models for single and double lid cavity configurations. Akbarinia and Behzadmehr [25] conducted investigation on mixed convection of a nanofluid consisting of alumina water in a horizontal curved tube numerically. The result shows that buoyancy force has a negative influence on the Nusselt number for particular Reynolds number, whereas the concentration of nanoparticles has a positive effect on the enhancement of heat transfer. Alinia et al. [26] investigated mixed convection of a nanofluid consisting of water and SiO_2 in an inclined enclosure cavity with the left and right walls maintained at different constant temperatures with moving lids and the upper and bottom walls. They concluded that the inclusion of nanoparticles greatly increases heat transfer in the cavity and induces major flow pattern changes. Shariat et al. [27] conducted research on laminar mixed convection alumina water nanofluid flow in elliptic ducts with constant heat flux boundary by employing two phase mixture model. Results show that increasing solid nanoparticles volume fraction increases the Nusselt number in a given Reynolds and Richardson number while the skin friction decreases.

Apart from application of nanofluid and type of cavities, the heat transfer and fluid flow in cavities having an inside body has received considerable attention in the recent years due to its practical engineering applications. Free convection in cavities having square inner solid is discussed in Alsabery et al. [28], Alsabery et al. [29], Mahmoodi

3

and Sebdani [30], and Sheremet et al. [31]. Alnajem et al. [32] considered the entropy generation and natural convection in a wavy-wall filled with a nanofluid and containing solid inner cylinder with isothermal heat source at the left vertical wall and adiabatic at the horizontal wall, while the right wavy wall cooled isothermally. Their outcome indicates that the influence of the addition of nanoparticles on the rate of heat transfer rate is necessary for low Rayleigh number and number of undulations. Alsabery et al. [33] investigated the time dependent mixed convection of alumina water nanoliquid in a differentially heated chamber with wavy upper wall and centered solid heat-conducting cylinder. They discovered that increase in the average Nusselt number at the hot wall depends on the moving parameter and the inner solid cylinder diameter. Selimefendigil et al. [34] numerically examined the mixed convection in a lid driven 3D flexible walled trapezoidal cavity with nanofluid. They observed that the differences in the Richardson number, elastic modulus of the side wall, and nanoparticle volume fraction for various side wall inclination angles of the trapezoidal cavity influenced the heat transfer and fluid flow characteristics. Liao and Lin [35] investigated mixed convection in a square enclosure with an isothermally rotating circular cylinder. It has been observed that the heat transfer changer according to the Rayleigh number, the aspect ratio and Prandtl number. The mixed convection and entropy generation in alumina-water nanofluid filling a wavy walled cavity containing a rotating conductive cylinder was investigated by Alsabery et al. [36]. They discovered that the cylinders rotation raises the rate of heat exchange at some Rayleigh number and increases with the volume fraction of the nanoparticles and the length of the heater segment. Rahman et al. [37] investigated the mixed convection in a two dimensional rectangular cavity with a uniform heat source applied on the right vertical wall where a circular heat conducting horizontal cylinder is placed within the cavity. It is shown that both rate of heat transfer from the heated wall and the dimensionless temperature in the cavity was highly dependent on the systems governing parameters and configurations studied, such as size, location, thermal conductivity of the cylinder and position of the inflow and outflow opening. Rahman and Alim [38] performed a research on the influence of magnetohydrodynamic (MHD) mixed convection flow in a vertical lid driven square enclosure including a heat conducting horizontal circular cylinder with joule heating. The investigation on the MHD mixed convection of Cu-water nanofluid filled triangular enclosure with a rotating cylinder was conducted by Shariat et al. [39]. Heat transfer and total entropy generation are shown to increase as the solid volume fraction of the nanoparticle increases. Rahman et al. [40] invesigated the effects of cylinder size and Richardson number on mixed convection flow inside a vented square cavity with a heat conducting horizontal solid circular cylinder placed at the center of the cavity. The results show that the streamlines, isotherms, average Nusselt number on the heated surface, average temperature of the fluid in the cavity and the dimensionless temperature in the center of the cylinder strongly depend on both the Richardson number and the cylinder diameter. Chatterjee et al. [41] conducted research on the mixed convective transport of $Cu-H_2O$ nanofluid in a differentially heated and lid driven square enclosure in the presence of a rotating and thermally insulated circular cylinder placed centrally within the enclosure. They found that the heat transfer rate is substantially affected by the rotational speed of the cylinder, mixed convective strength and the nanoparticle concentration. Billah et al. [42] investigated the mixed convection heat transfer in a lid driven cavity along with a heated circular hollow cylinder positioned at the center of the cavity. The result shows that the flow field and temperature distribution strongly depend on the cylinder diameter.

According to above mentioned studies and to the authors best knowledge, so far, there is no study being done on entropy generation and mixed convection of nanofluids in a lid driven trapezoidal cavity with different located solid cylinder. Gangawane et al. [43]

4

conducted mixed convection characteristic in a lid driven cavity with different locations and block sizes. It is shown that the heat transfer and fluid flow characteristics are more predominately affected byy size of block. A paper by Hussain and Hussein [44] studied mixed convection in a circular cylinder where isothermal temperature of the left side wall is higher than that of the opposite right-side wall while the upper and lower enclosure walls are adiabatic. They found that the rotating cylinder locations have an important effect in enhancing convection heat transfer in the square enclosure. Alsabery et al. [45] investigated mixed convection based on Buongiornos two phase model in a double lid driven square cavity including a solid inner body with alumina water. The top horizontal wall moves to the right and fixed at low temperature while the bottom horizontal walls is fixed at high temperature and moves to the left. Two of its governing parameters are the inner solid location and size of the inner solid. They discovered that a big size solid body can augment heat transfer in the case of high values of both Reynolds and Richardson numbers. The aim of this study is to investigate the impacts of differently located solid cylinder on entropy generation and mixed convection of nanofluids in a lid-driven trapezoidal cavity. Thus, it believed that this work is valuable.

2 Mathematical Formulation

Two-dimensional geometric model of mixed convection flow and heat transfer inside a trapezoidal cavity with bottom wall of length L and top wall with range $L/2$, with an internal solid cylinder with dimensional radius r that located in different locations as described schematically in Figure 1. The bottom surface assumed to be heated into a constant temperature of T_h, and the top surface slide with uniform velocity from left to right at $+U$ and preserved at a constant cold temperature, T_c. Meanwhile, both sloping surfaces with length $0.65L$ and inclination angle φ are saved in adiabatic rule. The fluid flow in the trapezoidal cavity is examined to hold steady, laminar, and loaded with an alumina-water nanofluids. The governing equations of Navier-Stokes equations and the energy equations toward the viscous incompressible flow can indicate into the dimensional model as the following:

$$\frac{\partial u}{\partial x} + \frac{\partial v}{\partial y} = 0 \tag{1}$$

$$u\frac{\partial u}{\partial x} + v\frac{\partial u}{\partial y} = -\frac{1}{\rho_{nf}}\frac{\partial p}{\partial x} + \nu_{nf}\left(\frac{\partial^2 u}{\partial x^2} + \frac{\partial^2 u}{\partial y^2}\right)$$

$$u\frac{\partial v}{\partial x} + v\frac{\partial v}{\partial y} = -\frac{1}{\rho_{nf}}\frac{\partial p}{\partial y} + \nu_{nf}\left(\frac{\partial^2 v}{\partial x^2} + \frac{\partial^2 v}{\partial y^2}\right) + \beta_{nf}\,g(T - T_0) \tag{2}$$

$$u\frac{\partial T}{\partial x} + v\frac{\partial T}{\partial y} = \alpha_{nf}\left(\frac{\partial^2 T}{\partial x^2} + \frac{\partial^2 T}{\partial y^2}\right) \tag{3}$$

The heat equation of the solid inner body remains as:

$$\frac{\partial^2 T_s}{\partial x^2} + \frac{\partial^2 T_s}{\partial y^2} = 0, \tag{4}$$

where x and y are the Cartesian coordinates measured in the horizontal and vertical directions respectively, g is the acceleration due to gravity, ρ_{nf} is the density of the nanofluid and ν_{nf} is the kinematic viscosity of the nanofluid. The thermo-physical properties of the nanofluid including heat capacitance $(\rho C_p)_{nf}$, effective thermal diffusivity α_{nf}, effective density ρ_{nf}, thermal expansion coefficient β_{nf}, can be explained respectfully as the
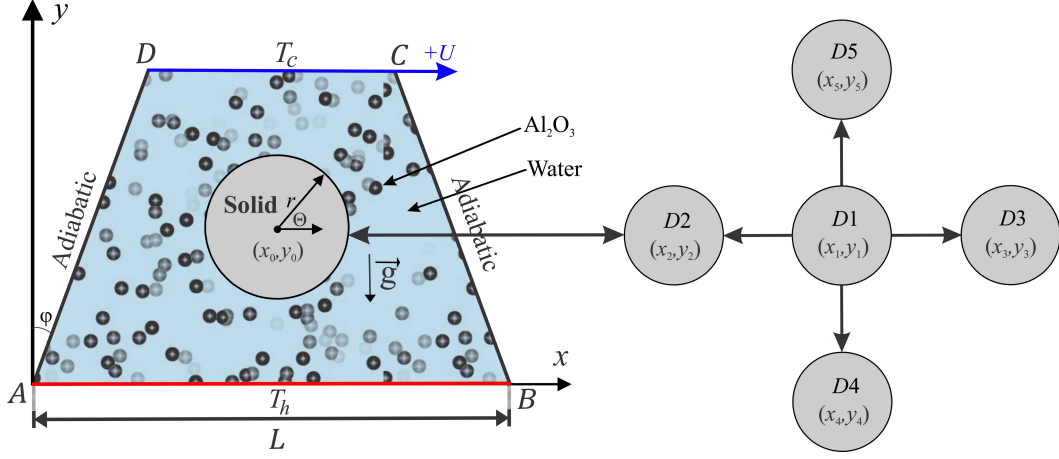
Figure 1: Physical model of convection in a trapezoidal cavity together with conducting wall and coordinate system.

following:

$$(\rho C_p)_{nf} = (1 - \phi)(\rho C_p)_f + \phi(\rho C_p)_p, \tag{5}$$

$$\alpha_{nf} = \frac{k_{nf}}{(\rho C_p)_{nf}}, \tag{6}$$

$$\rho_{nf} = (1 - \phi)\rho_f + \phi\rho_p, \tag{7}$$

$$(\rho\beta)_{nf} = (1 - \phi)(\rho\beta)_f + \phi(\rho\beta)_p. \tag{8}$$

While the dynamic viscosity ratio of water-Al$_2$O$_3$ nanofluids for 33nm particle-size in the ambient condition is described by Corcione [46] as follows.

$$\frac{\mu_{nf}}{\mu_f} = 1 / \left(1 - 34.87 \, (d_p/d_f)^{-0.3} \, \phi^{1.03} \right). \tag{9}$$

And the thermal conductivity ratio of water-Al$_2$O$_3$ nanofluids is calculated by Corcione [46] as the following:

$$\frac{k_{nf}}{k_f} = 1 + 4.4 \text{Re}_B^{0.4} \text{Pr}^{0.66} \left(\frac{T}{T_{fr}} \right)^{10} \left(\frac{k_p}{k_f} \right)^{0.03} \phi^{0.66}. \tag{10}$$

Where Re$_B$ is defined as

$$\text{Re}_B = \frac{\rho_f u_B d_p}{\mu_f}, \quad u_B = \frac{2k_b T}{\pi \mu_f d_p^2}. \tag{11}$$

Where $k_b = 1.380648 \times 10^{-23}(J/K)$ is the Boltzmann constant. $l_f = 0.17$nm is the mean path of fluid particles. d_f is the molecular diameter of water given as Corcione [46]

$$d_f = \frac{6M}{N\pi\rho_f}. \tag{12}$$

Where M is the molecular weight of the base fluid, N is the Avogadro number and ρ_f is the density of the base fluid at standard temperature (310K).

Now we introduce the following non-dimensional variables:

$$X = \frac{x}{L}, \quad Y = \frac{y}{L}, \quad U = \frac{u}{U_0}, \quad V = \frac{v}{U_0}, \quad \theta = \frac{T - T_c}{T_h - T_c}, \quad \theta_s = \frac{T_s - T_c}{T_h - T_c},$$

$$D = \frac{d}{L}, \quad \text{Pr} = \frac{\nu_f}{\alpha_f}, \quad P = \frac{pL^2}{\rho_f \alpha_f^2} \tag{13}$$

6

This then yields the dimensionless governing equations are:

$$\frac{\partial U}{\partial X} + \frac{\partial V}{\partial Y} = 0 \tag{14}$$

$$U\frac{\partial U}{\partial X} + V\frac{\partial U}{\partial Y} = -\frac{\partial P}{\partial X} + \frac{1}{Re}\frac{\rho_f}{\rho_{nf}}\frac{\mu_{nf}}{\mu_f}\left(\frac{\partial^2 U}{\partial x^2} + \frac{\partial^2 U}{\partial Y^2}\right) \tag{15}$$

$$U\frac{\partial V}{\partial X} + V\frac{\partial V}{\partial Y} = -\frac{\partial P}{\partial Y} + \frac{1}{Re}\frac{\rho_f}{\rho_{nf}}\frac{\mu_{nf}}{\mu_f}\left(\frac{\partial^2 V}{\partial X^2} + \frac{\partial^2 V}{\partial Y^2}\right) + \frac{(\rho\beta)_{nf}}{\rho_{nf}\beta_f}\frac{Gr}{Re^2}\theta \tag{16}$$

$$U\frac{\partial \theta}{\partial X} + V\frac{\partial \theta}{\partial Y} = \frac{\alpha_{nf}}{\alpha_f}\frac{1}{Pr\,Re}\left(\frac{\partial^2 \theta}{\partial X^2} + \frac{\partial^2 \theta}{\partial Y^2}\right), \tag{17}$$

$$\frac{\partial^2 \theta_s}{\partial x^2} + \frac{\partial^2 \theta_s}{\partial y^2} = 0, \tag{18}$$

where $Ri = \frac{Gr}{Re^2}$ shows the Richardson number. The dimensionless boundary conditions regarding Eqs. (14) and (18) are:

On the bottom heated surface (AB):
$$U = V = 0, \ \ \theta = 1, \ \ 0 \le X \le 1, \ \ Y = 0, \tag{19}$$
On the top moving cold surface (DC):
$$U = 1, V = 0, \ \ \theta = 0, \ \ 0 \le X \le 1, \ \ Y = 0.65, \tag{20}$$
On the left and right sloping surfaces (AD and BC):
$$U = V = 0, \ \ \frac{\partial \theta}{\partial(X,Y)} = 0, \ \ \forall X, \ \ \forall Y, \tag{21}$$
$$\theta = \theta_s, \ \ \text{at the outer solid cylinder surface,} \tag{22}$$
$$U = V = 0, \ \ \frac{\partial \theta}{\partial n} = K_r \frac{\partial \theta_s}{\partial n}, \tag{23}$$

where $K_r = k_s/k_{nf}$ keeps the thermal conductivity ratio above the covering of the internal body. The local Nusselt number evaluated at the heated bottom horizontal surface, which is defined by

$$Nu_{nf} = -\left(\frac{\partial \theta}{\partial X}\right)_{Y=0}, \tag{24}$$

Finally, the average Nusselt number evaluated at the heated part of the bottom horizontal surface of the cavity which is given by:

$$\overline{Nu}_{nf} = \int_A^B Nu_{nf}\, \mathrm{d}Y, \tag{25}$$

The entropy generation relation is given by [47, 48]:

$$S = \frac{k_{nf}}{T_0^2}\left[\left(\frac{\partial T}{\partial x}\right)^2 + \left(\frac{\partial T}{\partial y}\right)^2\right] + \frac{\mu_{nf}}{T_0}\left[2\left(\frac{\partial u}{\partial x}\right)^2 + 2\left(\frac{\partial v}{\partial y}\right)^2 + \left(\frac{\partial u}{\partial x} + \frac{\partial v}{\partial x}\right)^2\right]. \tag{26}$$

In dimensionless form, local entropy generation can be expressed as:

$$S_{\text{GEN}} = \frac{k_{nf}}{k_f}\left[\left(\frac{\partial \theta}{\partial X}\right)^2 + \left(\frac{\partial \theta}{\partial Y}\right)^2\right]$$
$$+ \frac{\mu_{nf}}{\mu_f}N_\mu\left\{2\left[\left(\frac{\partial U}{\partial X}\right)^2 + \left(\frac{\partial V}{\partial Y}\right)^2\right] + \left(\frac{\partial^2 U}{\partial Y^2} + \frac{\partial^2 V}{\partial X^2}\right)^2\right\}, \tag{27}$$

where, $N_\mu = \frac{\mu_f T_0}{k_f}\left(\frac{\alpha_f}{L(\Delta T)}\right)^2$ is the irreversibility distribution ratio and $S_{\text{GEN}} = S_{gen}\frac{T_0^2 L^2}{k_f(\Delta T)^2}$.

The terms of Eq. (27) can be separated to the following form:

$$S_{\text{GEN}} = S_\theta + S_\Psi, \tag{28}$$

where S_θ and S_Ψ are the entropy generation due to heat transfer irreversibility (HTI) and fluid friction irreversibility (FFI), respectively.

$$S_\theta = \frac{k_{nf}}{k_f} \left[\left(\frac{\partial \theta}{\partial X} \right)^2 + \left(\frac{\partial \theta}{\partial Y} \right)^2 \right], \tag{29}$$

$$S_\Psi = \frac{\mu_{nf}}{\mu_f} N_\mu \left\{ 2 \left[\left(\frac{\partial U}{\partial X} \right)^2 + \left(\frac{\partial V}{\partial Y} \right)^2 \right] + \left(\frac{\partial^2 U}{\partial Y^2} + \frac{\partial^2 V}{\partial X^2} \right)^2 \right\}. \tag{30}$$

By Integrating Eq. (28) over the domain, the global entropy generation (GEG) for the present two-dimensional study is obtained as the following:

$$\text{GEG} = \int S_{GEN} \, \mathrm{d}X\mathrm{d}Y = \int S_\theta \, \mathrm{d}X\mathrm{d}Y + \int S_\Psi \, \mathrm{d}X\mathrm{d}Y. \tag{31}$$

It is appropriate to mention Bejan number in order to determine which is the dominant, heat transfer or fluid friction irreversibility. Bejan number is defined as:

$$Be = \frac{\int S_\theta \, \mathrm{d}X\mathrm{d}Y}{\int S_{GEN} \, \mathrm{d}X\mathrm{d}Y}. \tag{32}$$

When $Be > 0.5$, the HTI is the dominant, while when $Be < 0.5$, the FFI is the dominant.

3   Numerical Method and Validation

The Galerkin weighted residual along with finite element methods are employed to investigate the control equations (14)–(18) subject to the boundary conditions Eqs. (19)–(23). The finite element analysis of the momentum equations (15) and (16) is showing by the following procedure:

Primary, we apply the penalty finite element method by excluding the pressure (P) including a penalty parameter (λ) as the following:

$$P = -\lambda \left(\frac{\partial U}{\partial X} + \frac{\partial V}{\partial Y} \right).$$

Leads to the following momentum equations toward the X and Y-directions:

$$U \frac{\partial U}{\partial X} + V \frac{\partial U}{\partial Y} = \frac{\partial \lambda}{\partial X} \left(\frac{\partial U}{\partial X} + \frac{\partial V}{\partial Y} \right) + \frac{\rho_f}{\rho_{nf}} \frac{\mu_{nf}}{\mu_f} \frac{1}{Re} \left(\frac{\partial^2 U}{\partial X^2} + \frac{\partial^2 U}{\partial Y^2} \right),$$

$$U \frac{\partial V}{\partial X} + V \frac{\partial V}{\partial Y} = \frac{\partial \lambda}{\partial Y} \left(\frac{\partial U}{\partial X} + \frac{\partial V}{\partial Y} \right) + \frac{\rho_f}{\rho_{nf}} \frac{\mu_{nf}}{\mu_f} \frac{1}{Re} \left(\frac{\partial^2 V}{\partial X^2} + \frac{\partial^2 V}{\partial Y^2} \right) + \frac{(\rho\beta)_{nf}}{\rho_{nf}\beta_f} \frac{Gr}{Re^2} \theta_{nf}.$$

The weak (or weighted-integral) formulation regarding the momentum equations by multiplying the equation by an internal domain (Φ) and integrating it over the computational domain which is discretised toward small triangular elements as revealed in Fig. 2. The following weak formulations are obtained:

$$\int_\Omega \left(\Phi_i U^k \frac{\partial U^k}{\partial X} + \Phi_i V^k \frac{\partial U^k}{\partial Y} \right) \mathrm{d}X\mathrm{d}Y = \lambda \int_\Omega \frac{\partial \Phi_i}{\partial X} \left(\frac{\partial U^k}{\partial X} + \frac{\partial V^k}{\partial Y} \right) \mathrm{d}X\mathrm{d}Y$$

$$+\frac{\rho_f}{\rho_{nf}}\frac{\mu_{nf}}{\mu_f}\frac{1}{Re}\int_\Omega \Phi_i\left(\frac{\partial^2 U^k}{\partial X^2}+\frac{\partial^2 U^k}{\partial Y^2}\right)\mathrm{dXdY},$$

$$\int_\Omega\left(\Phi_i V^k\frac{\partial V^k}{\partial X}+\Phi_i V^k\frac{\partial V^k}{\partial Y}\right)\mathrm{dXdY}=\lambda\int_\Omega\frac{\partial\Phi_i}{\partial Y}\left(\frac{\partial U^k}{\partial X}+\frac{\partial V^k}{\partial Y}\right)\mathrm{dXdY}$$

$$+\frac{\rho_f}{\rho_{nf}}\frac{\mu_{nf}}{\mu_f}\frac{1}{Re}\int_\Omega \Phi_i\left(\frac{\partial^2 V^k}{\partial X^2}+\frac{\partial^2 V^k}{\partial Y^2}\right)\mathrm{dXdY}+\frac{(\rho\beta)_{nf}}{\rho_{nf}\beta_f}\frac{Gr}{Re^2}\int_\Omega \Phi_i\theta_{nf}^k\mathrm{dXdY}.$$

Selection about the interpolation functions as implementing an approximation toward the velocity distribution and temperature distribution as:

$$U\approx\sum_{j=1}^m U_j\Phi_j(X,Y),\quad V\approx\sum_{j=1}^m V_j\Phi_j(X,Y),\quad \theta\approx\sum_{j=1}^m \theta_j\Phi_j(X,Y).$$

The nonlinear residual equations for the momentum equations that obtained from the Galerkin weighted residual finite-element method are:

$$R(1)_i=\sum_{j=1}^m U_j\int_\Omega\left[\left(\sum_{j=1}^m U_j\Phi_j\right)\frac{\partial\Phi_j}{\partial X}+\left(\sum_{j=1}^m V_j\Phi_j\right)\frac{\partial\Phi_j}{\partial Y}\right]\Phi_i\mathrm{dXdY}$$

$$+\lambda\left[\sum_{j=1}^m U_j\int_\Omega\frac{\partial\Phi_i}{\partial X}\frac{\partial\Phi_j}{\partial X}\mathrm{dXdY}+\sum_{j=1}^m V_j\int_\Omega\frac{\partial\Phi_i}{\partial X}\frac{\partial\Phi_j}{\partial Y}\mathrm{dXdY}\right]$$

$$+\frac{\rho_f}{\rho_{nf}}\frac{\mu_{nf}}{\mu_f}\frac{1}{Re}\sum_{j=1}^m U_j\int_\Omega\left[\frac{\partial\Phi_i}{\partial X}\frac{\partial\Phi_j}{\partial X}+\frac{\partial\Phi_i}{\partial Y}\frac{\partial\Phi_j}{\partial Y}\right]\mathrm{dXdY},$$

$$R(2)_i=\sum_{j=1}^m V_j\int_\Omega\left[\left(\sum_{j=1}^m U_j\Phi_j\right)\frac{\partial\Phi_j}{\partial X}+\left(\sum_{j=1}^m V_j\Phi_j\right)\frac{\partial\Phi_j}{\partial Y}\right]\Phi_i\mathrm{dXdY}$$

$$+\lambda\left[\sum_{j=1}^m U_j\int_\Omega\frac{\partial\Phi_i}{\partial Y}\frac{\partial\Phi_j}{\partial X}\mathrm{dXdY}+\sum_{j=1}^m V_j\int_\Omega\frac{\partial\Phi_i}{\partial Y}\frac{\partial\Phi_j}{\partial Y}\mathrm{dXdY}\right]$$

$$+\frac{\rho_f}{\rho_{nf}}\frac{\mu_{nf}}{\mu_f}\frac{1}{Re}\sum_{j=1}^m V_j\int_\Omega\left[\frac{\partial\Phi_i}{\partial X}\frac{\partial\Phi_j}{\partial X}+\frac{\partial\Phi_i}{\partial Y}\frac{\partial\Phi_j}{\partial Y}\right]\mathrm{dXdY}$$

$$+\frac{(\rho\beta)_{nf}}{\rho_{nf}\beta_f}\frac{Gr}{Re^2}\int_\Omega\left(\sum_{j=1}^m \theta_j\Phi_j\right)\Phi_i\mathrm{dXdY},$$

where the superscript k is the relative index, subscripts i, j and m are the residual number, node number and iteration number, respectively. For clarifying the nonlinear terms into the momentum equations, a Newton-Raphson iteration algorithm was employed. The convergence of the solution is allowed through the relative error to any of the variables does satisfy the resulting convergence criteria:

$$\left|\frac{\Gamma^{m+1}-\Gamma^m}{\Gamma^{m+1}}\right|\le 10^{-5}.$$

For the purpose of validating the data, we have compared the present results with the previous numerical findings that presented by Khanafer and Aithal [49] for the problem of free convective flow and heat transfer in a square cavity that filled with pure fluid and partially heated from below, as explained in Figs. 3 and 4. In addition, a comparison is made between the resulting figures and the one provided by Ilis et al. [47] for the case
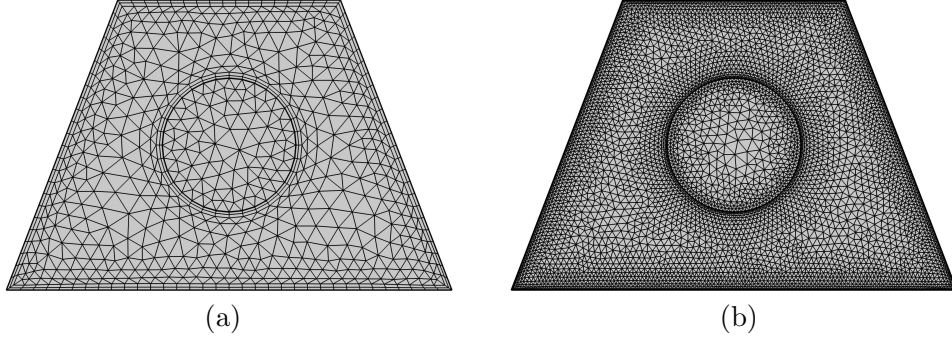
Figure 2: Grid-points distribution for the grid size of (a) 1339 and (b) 9846 elements.

Table 1: Thermo-physical properties of water with Al_2O_3 nanoparticles at $T = 310K$ [53].

Physical properties	Fluid phase (water)	Al_2O_3
C_p (J/kgK)	4178	765
ρ (kg/m^3)	993	3970
k (Wm^{-1}K^{-1})	0.628	40
$\beta \times 10^5$ (1/K)	36.2	0.85
$\mu \times 10^6$ (kg/ms)	695	–
d_p (nm)	0.385	33

of entropy generation and natural convection in a square cavity fully heated from sides, as shown in Fig. 5. Figure 6 shows alternative comparisons regarding the enhancement in the thermal conductivity due to the addition of the Al_2O_3 nanoparticles with two different experimental results and the numerical results of Corcione et al. [50] as well. These results provide confidence to the accuracy of the present numerical method.

4   Results and Discussion

In this part, we present numerical results concerning the streamlines, isotherms and isentropic lines (the local dimensionless entropy generation) with various values of Richardson number ($0.01 \leq Ri \leq 10$), Reynolds number ($5 \leq Re \leq 500$), nanoparticles volume fraction ($0 \leq \phi \leq 0.04$), dimensionless radius of solid cylinder ($0.05 \leq S \leq 0.25$) and dimensionless location of solid cylinder (D) [$D1 = (X = 0.5, Y = 0.5), D2 = (X = 0.35, Y = 0.5), D3 = (X = 0.65, Y = 0.5), D4 = (X = 0.5, Y = 0.2), D5 = (X = 0.5, Y = 0.45)$]. Values of Prandtl number, thermal conductivity of the solid cylinder and side surface inclination angle are fixed at Pr = 4.623, $k_s = 0.76$ and $\varphi = 22.5°$. The thermophysical properties of the used base fluid (water) and solid Al_2O_3 phases are described in Table 1.

Figure 7 shows distributions of streamlines, isotherms and isentropic lines for different values of Richardson number for $\phi = 0.02$, $R = 0.15$, $Re = 100$ and the inner solid located at the center of the solid. Therefore, an increase in Ri is due a growth of Grashof number. Natural convection is negligible if Richardson number is less than 1.0. Due to the motion direction of the upper wall, one small cell appear at the top of the solid wall
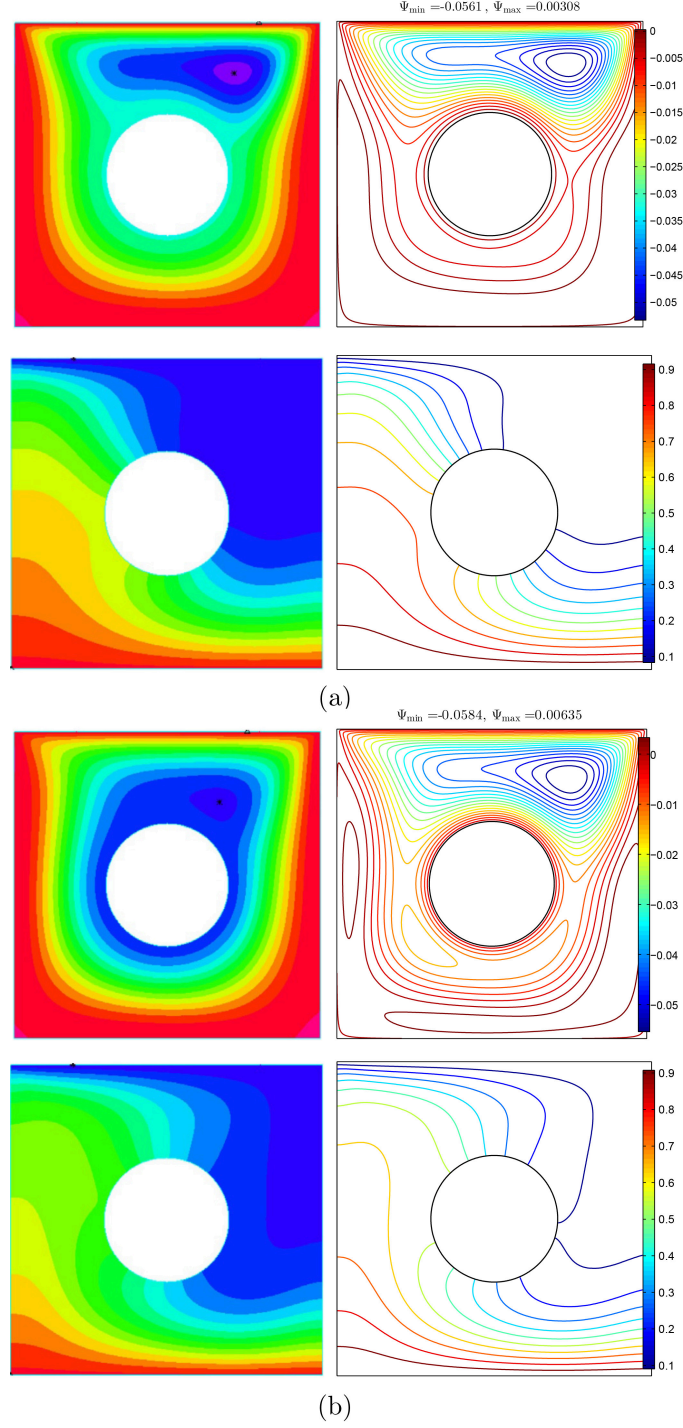
10

Figure 3: (left) Khanafer and Aithal [49] and (right) present study for (a) streamlines at $Ra = 10^6$ and $H = 0.4$, (b) isotherms at $Ra = 10^5$ and $H = 0.8$ and (c) isotherms at $Ra = 1.836 \times 10^5$ and $H = 0.8$ for the case of numerical and experimental results of Khanafer and Aithal [49] at $\phi = 0$ and $D = 0$.

in Fig. 7 (a) and (b). As Ri increase, the streamlines are extending downwards as in Fig. 7 (c) since both natural and forced convection exist. When the Ri increases to 10, multi cellular appear at the top of the wall as well as the bottom of the wall. Since the bottom wall is heated and the upper wall is cooled, the isotherm patterns appear with

11

Figure 4: Comparison of the average Nusselt number interface with Ra for different H with Khanafer and Aithal [49] at $\phi = 0$ and $D = 0$.

curved lines. We can see that the curved lines appear at the top left and the bottom right of the solid as in Fig. 7(a). There is no change in the isotherm patterns as Ri increase. But, at $Ri = 10$, the isotherm curved lines elongated to the right of the solid. The entropy regions produced by the heat transfer irreversibility (HTI) and the nanofluid flow irreversibility (NFI) that arise for high temperatures and the velocity gradients. The isentropic lines depict a concentrated entropy generation close to three regions, namely top and right bottom of the enclosure and surface of the solid cylinder. There is no change of the isentropic lines at smaller Ri number. Only at $Ri = 10$, the isentropic lines slightly change as the lines appear at the center bottom of the solid and the sloping surfaces wall.

Figure 8 shows the effect of variations Reynold number on streamlines, isotherm, and isentropic with $Ri = 1$, $\phi = 0.02$, $R = 0.15$. In Figure 8 (a) , the streamlines appear with 2 rotating cells at the top of the wall and one rotating cell at the bottom of the wall. The reason of this is the shear force and buoyant force dominate at smaller Reynolds number. As Re increases, the cell at bottom of the wall and top right shrink while the cell at top left expands as in Figure 8(b). Furthermore, the cell at top right and bottom do not exist while the cell at top left expands at higher Re as in Figure 8 (c) and (d). These happen because the velocity of the top lid increases as Reynolds number increase. Since the velocity of the top lid increased, forced convection dominates compared to the buoyant force. Since the cooling activity occurs at the top wall while the heating activity occurs at the bottom wall, thick thermal boundary layers clustered at the top left and bottom right of the cavity wall. The isotherms are approximately horizontal. Increase Re disturbs the isotherm inside the cavity. As $Re = 50$, we can see that the intensity of the isotherm patterns increased at the top left and bottom right walls and decreased at the right side of the cavity. Furthermore, intensity of the isotherm pattern decreased in the cavity as Re increases. The isentropic lines show a concentrated entropy generation inside the cavity and around the solid cylinder. These entropy regions result from the heat transfer irreversibility(HTI) and the nanofluid irreversibility (NFI) that arise from shear force and buoyant force. As Re increases, the intensity of isentropic lines decrease especially around the solid cylinder. When $Re = 500$, the isentropic lines only appear at the top and bottom of the wall. The reason why this happens is the intensity of isentropic lines are high at the top of the wall due to shear force dominate as Re increase.

Figure 9 depicts the local Nusselt number interface with X and local entropy generation at the outer cylinder surface for different Richardson number. Local Nusselt number
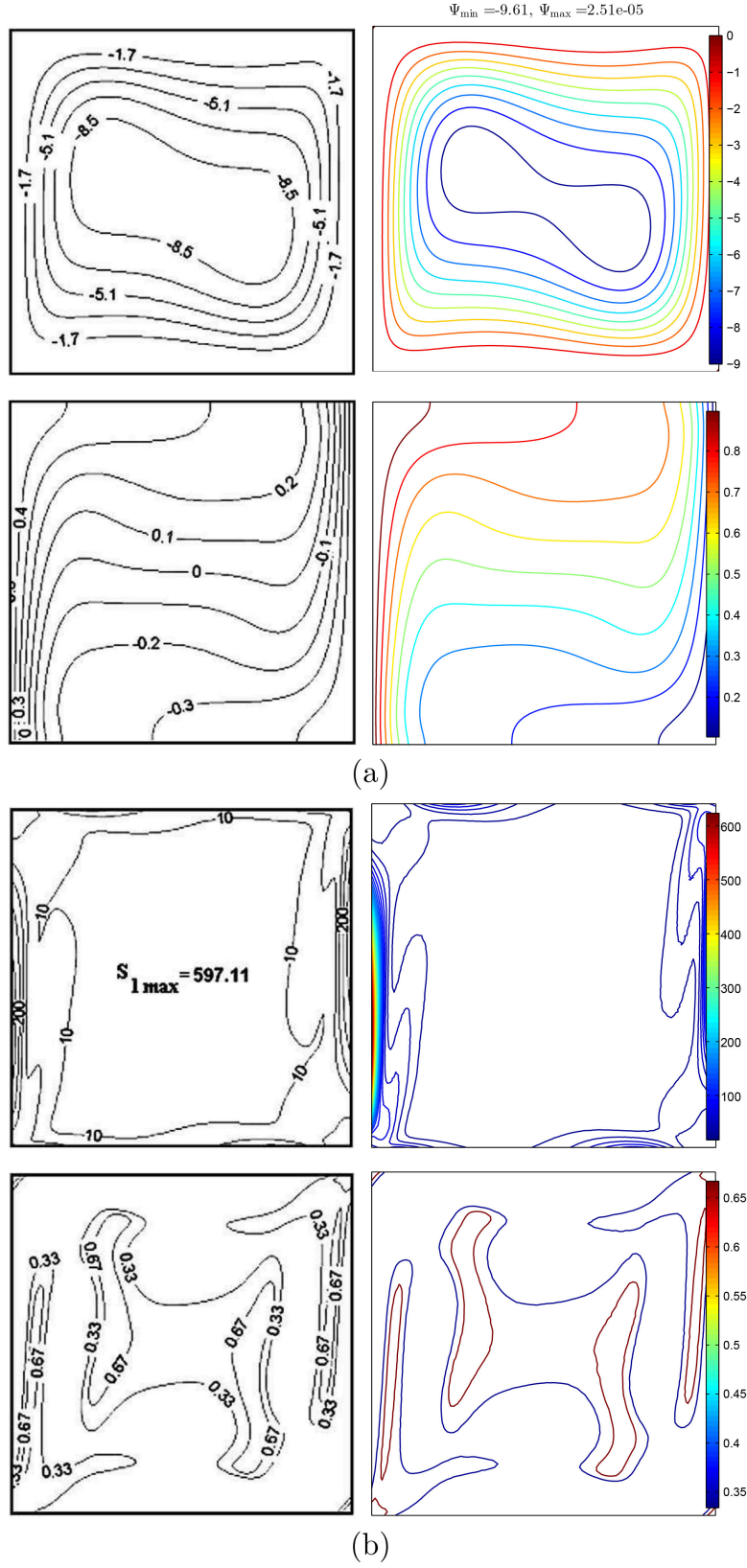
12

Figure 5: Streamlines and isotherms (a), global entropy generation and Bejan number (b), Ilis et al. [47] (left), present study (right), for $Ra = 10^5$, $\phi = 0$, D and $H = 1$.
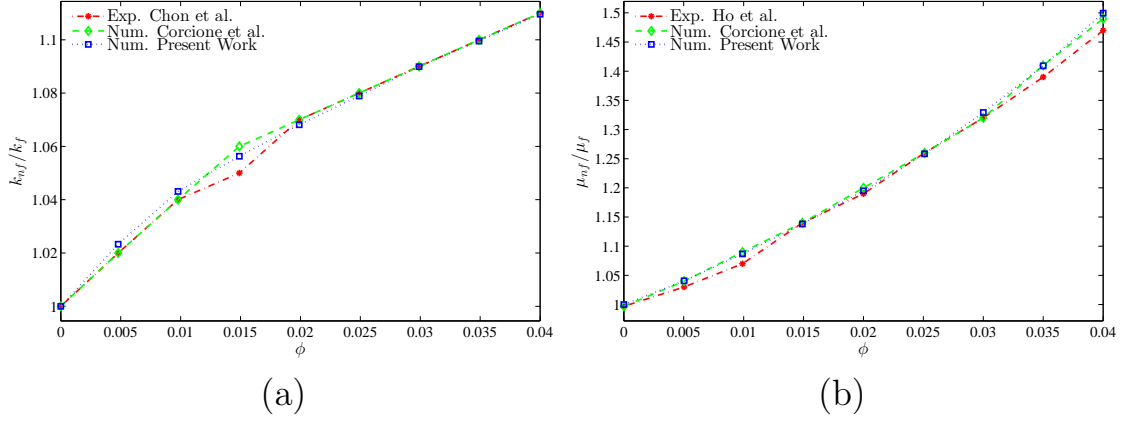
Figure 6: Comparison of (a) thermal conductivity ratio with Chon et al. [51] and Corcione et al. [50] and (b) dynamic viscosity ratio with Ho et al. [52] and Corcione et al. [50].

is maximum for all Richardson number at $X = 0.4$. The highest local Nusselt number is when $Ri = 10$ because the system is dominant with natural convection. At lowest Richardson number, we can see that the local entropy generation is highest at both vertical walls. Figure 10 depicts the distribution of the local Nusselt number, exhibits maximum heat transfer at $X = 0.4$ for all Reynolds number. Higher Reynold number gives maximum heat transfer compared to small Reynolds number.

Figure 12 illustrates the effect of different nanoparticle volume fraction on average Nusselt number, Bejan number and global entropy generation with Richardson number at $Re = 100$, $R = 0.15$ and the location of inner solid at the center of the enclosure.As Ri increases, the average Nusselt number also increase for all nanoparticles volume fraction. We observed that the best performance of the average Nusselt number is at higher nanoparticles volume fraction. Since the value of Be is close to 1, it shows that the system is heat tranfer irreversibility dominant compared to nanofluid irreversibility. The value of Be is decreases for all nanoparticle volume fraction. The system is forced convection dominant if Richardson number is small. As the system changed to natural convection, we can see that the GEG increases. Higher nanoparticle volume fraction gives best result for global entropy generation compared to smaller nanoparticle volume fraction.

Figure 12 depicts the effect of different nanoparticles volume fraction on the average Nusselt number, Bejan number and the global entropy generation with Reynolds number at $Ri = 1$, $R = 0.15$ and same position of inner solid as in Figure 11. Increase Re means we increase the velocity of the top lid. As Re increases, we can see that the average Nusselt number and GEG increase. The change of nanoparticle volume fraction also effect the average Nusselt number, Bejan and global entropy generation. We observed that the best performance for average Nusselt number and GEG is when the nanoparticle volume fraction is at 0.04. From graph, we noticed that the system is HTI dominant for all nanoparticle volume fraction. As Re increases to 50, we can see that the graph increases. However, the graph decreases when Re greater than 50, this may be due to combined of natural and forced convection.

The effect of various radius of cylinder on the streamlines, isotherms and isentropic are depicted in Figure 13 with $Ri = 1$, $Re = 100$, $\phi = 0.02$. As radius of cylinder increases, the passage width between the cylinder and the top and bottom wall decreases. Therefore, we can see that the size of cell decreases as the radius of cylinder increase.
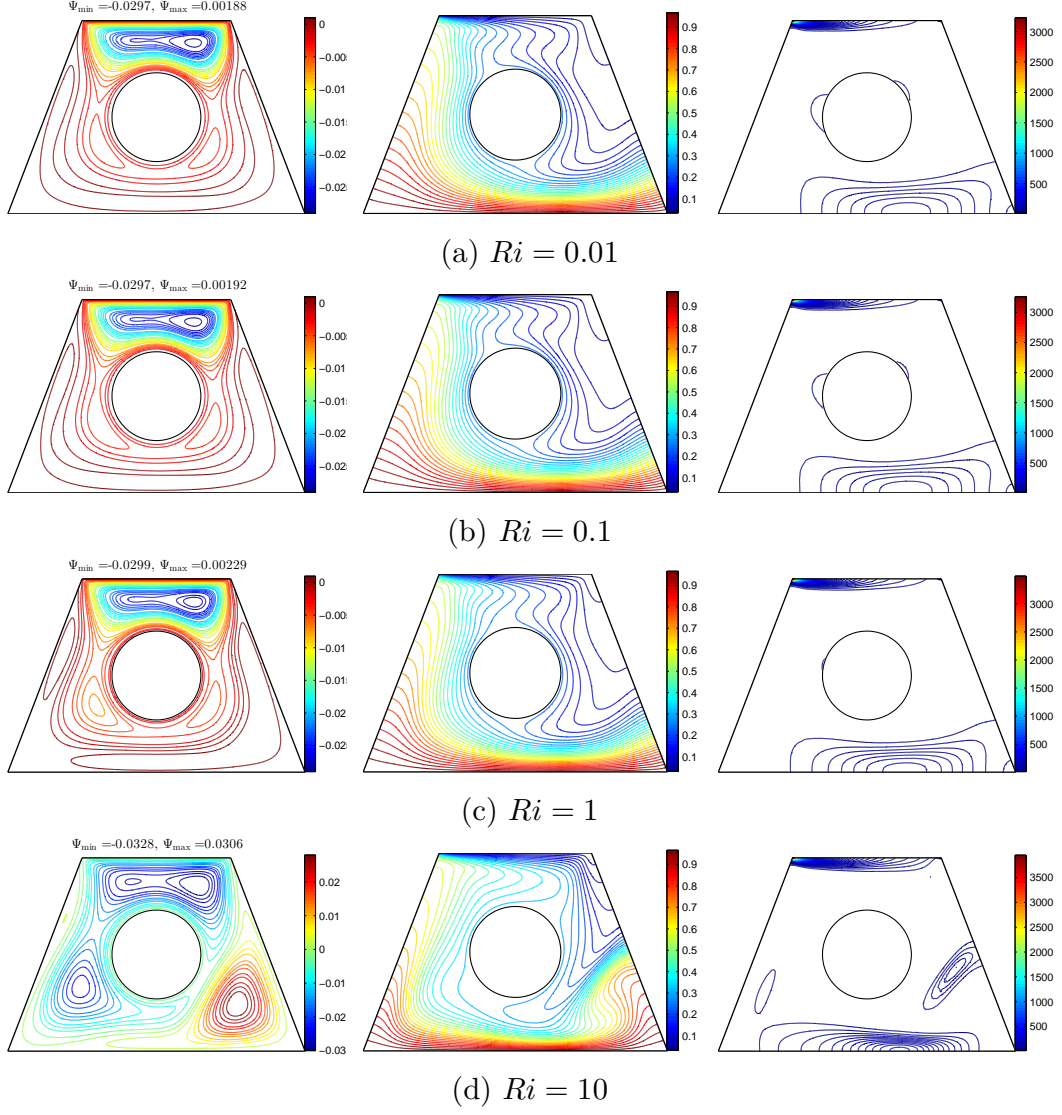
14

$\Psi_{\min} = -0.0297$, $\Psi_{\max} = 0.00188$

(a) $Ri = 0.01$

$\Psi_{\min} = -0.0297$, $\Psi_{\max} = 0.00192$

(b) $Ri = 0.1$

$\Psi_{\min} = -0.0299$, $\Psi_{\max} = 0.00229$

(c) $Ri = 1$

$\Psi_{\min} = -0.0328$, $\Psi_{\max} = 0.0306$

(d) $Ri = 10$

Figure 7: Variation of the streamlines (left), isotherms (middle), and isentropic (right) evolution by Richardson number (Ri) for $Re = 100$, $\phi = 0.02$, $R = 0.15$ and $D1$.
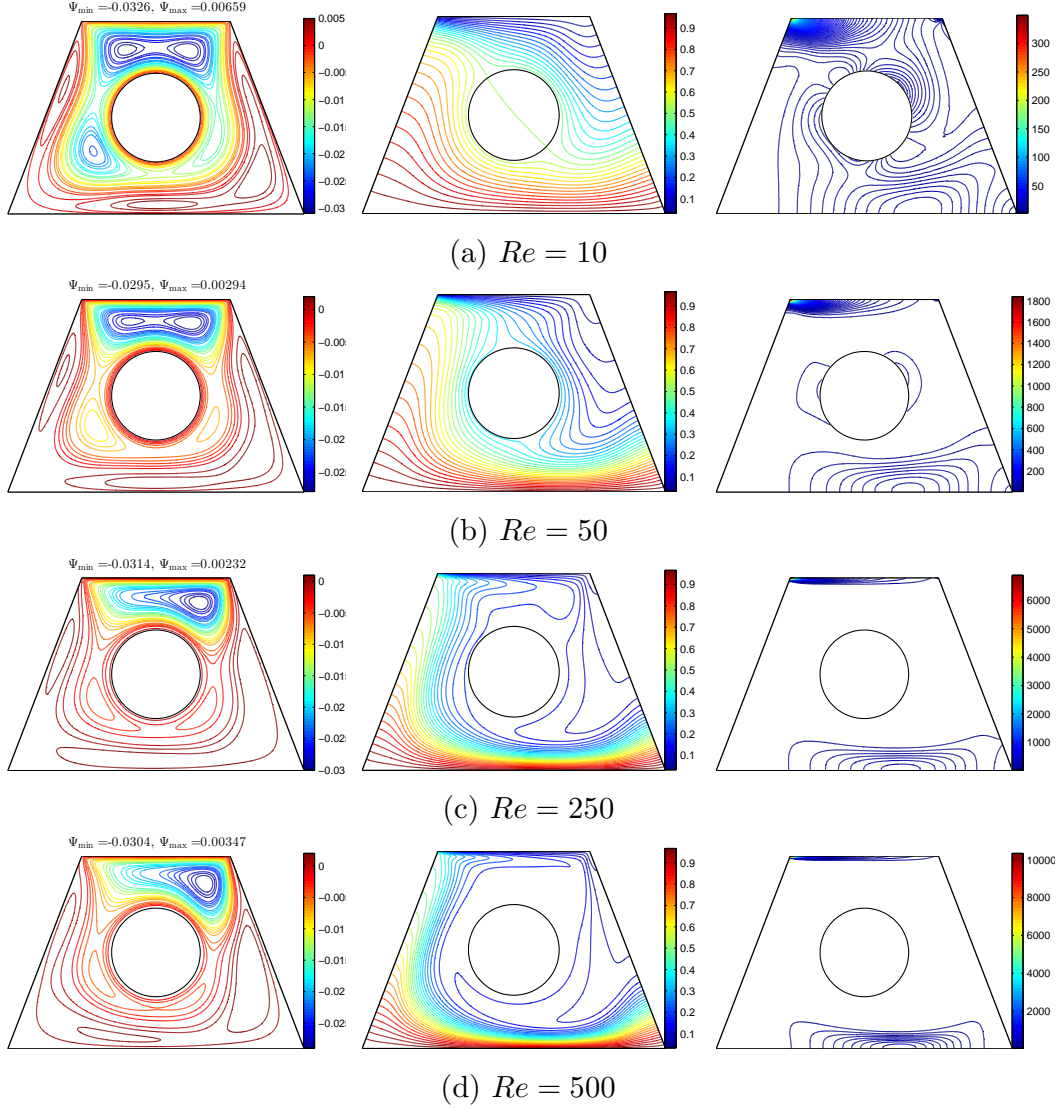
Figure 8: Variation of the streamlines (left), isotherms (middle), and isentropic (right) evolution by Reynolds number (Re) for $Ri = 1$, $\phi = 0.02$, $R = 0.15$ and $D1$.

Furthermore, there are two cells appear when radius of cylinder greater than 0.2. As a result, increase in the solid cylinder shows high intensity of isotherm lines at the bottom and top of the cavity. For small radius, it shows that the intensity of isentropic are similar which the isentropic lines appear at the top and bottom of the wall. Only at higher radius, the isentropic lines appear at the solid cylinder as well.

Figure 14 depicts the local Nusselt number interfaces with X and local entropy generation at the outer solid cylinder surface with different radius of solid cylinder. Figure 14 (a) shows that the maximum heat transfer occur mostly at the center of the cavity. Figure 14 (b) illustrates that the local entropy generation has no change at smaller radius of solid cylinder. The local entropy generation has sinusoidal shape for higher radius of solid cylinder.

It is found that the changes of radius of solid cylinder affects the average Nusselt number, Bejan number and global entropy generation as in Figure 15. The average Nusselt number in Figure 15 (a) and global entropy generation in Figure 15 (b) were
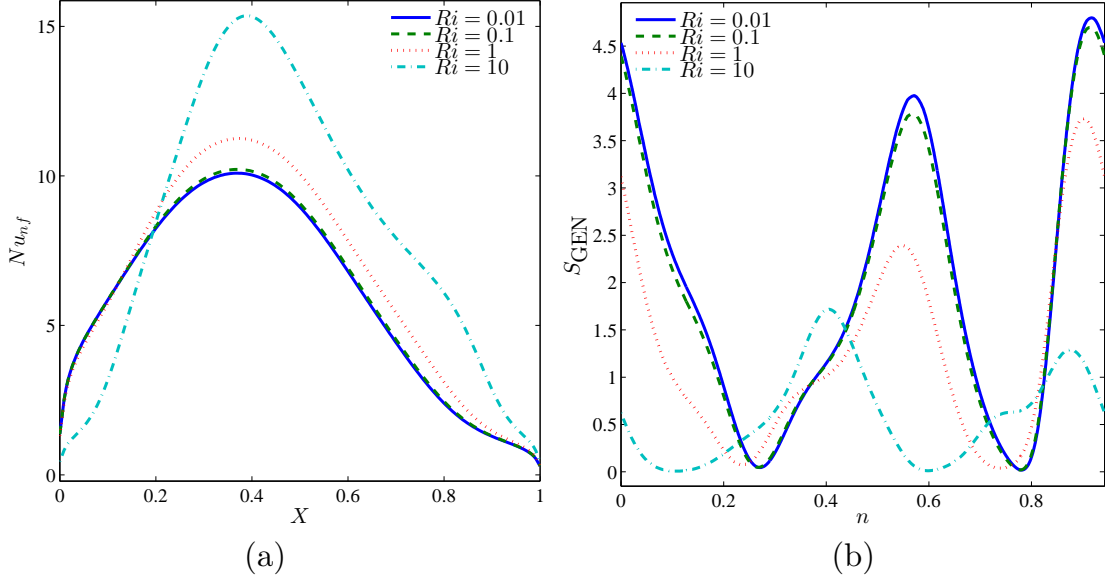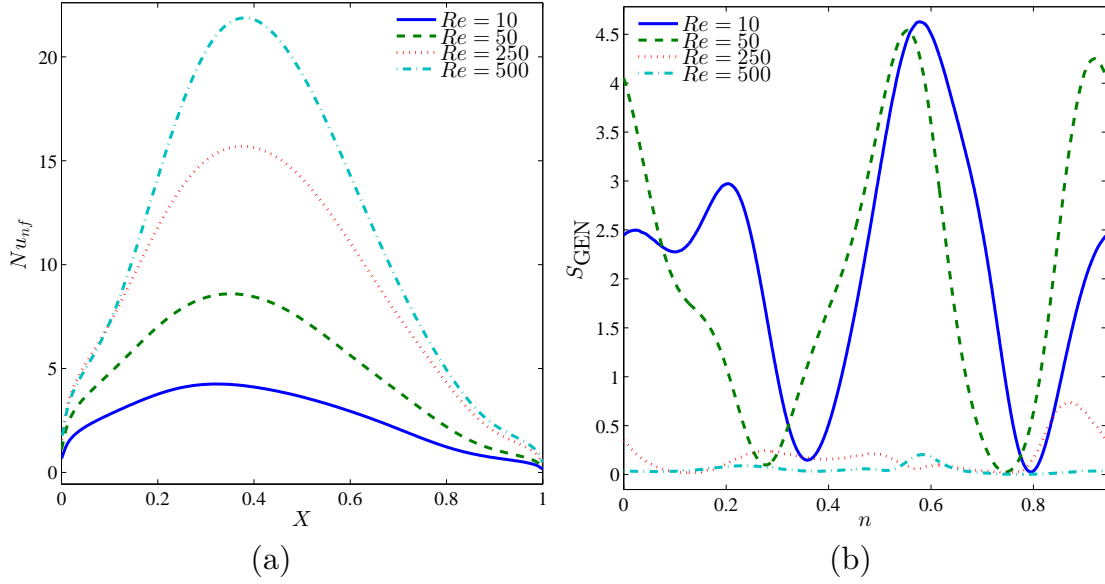
16

Figure 9: Variation of (a) local Nusselt number interfaces with X and (b) local entropy generation at the outer solid cylinder surface for different Ri at $Re = 100$, $\phi = 0.02$, $R = 0.15$ and $D1$.

Figure 10: Variation of (a) local Nusselt number interfaces with X and (b) local entropy generation at the outer solid cylinder surface for different Re at $Ri = 1$, $\phi = 0.02$, $R = 0.15$ and $D1$.

found to increase when Re number increase. This is probably due to the increase in the velocity of the top lid as Re increase, affecting thermal performance. Furthermore, the Bejan number are high for all radius and indicate that the system is HTI dominant as in Figure 15 (b). The graph illustrates that the Bejan number is increasing for all radius except $R = 0.25$ until $Re = 50$ and decreasing after that. This is because the fluid friction increases as Re increase and resulting Bejan number decrease.

Figure 16 illustrates the effect of various positions of solid cylinder on streamlines,
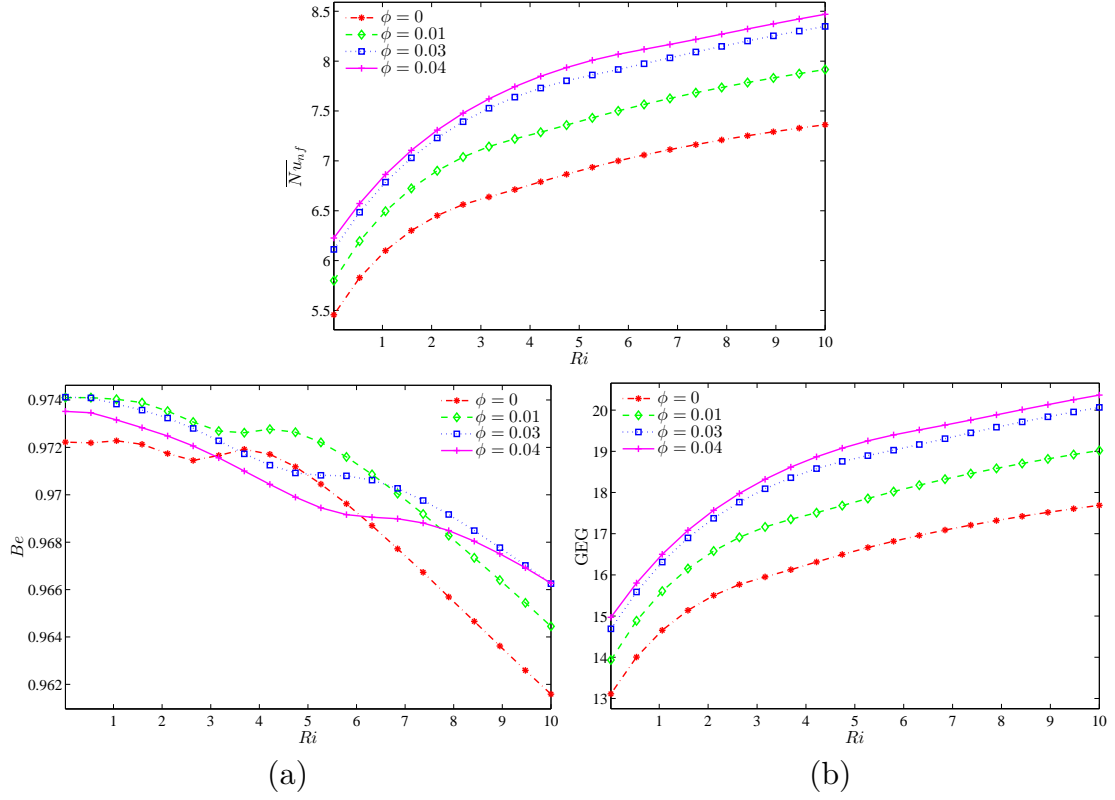
Figure 11: Variation of (a) average Nusselt number ($\overline{Nu}_{nf}$), (b) Bejan number (Be) and (c) the global entropy generation (GEG) with Ri for different values of ϕ at $Re = 100$, $R = 0.15$ and $D1$.

isotherm and isentropic with Richardson number, Reynolds number , nanoparticle volume fraction and radius of solid cyilnder are 1, 100, 0.02 and 0.15 respectively. In Fig. 16 (a) dan (b), the position of solid cylinder is kept constant at $y = 0.5$ but the value of x is different, where $x = 0.35$ and $x = 0.65$ respectively while in Fig. 16 (c) and (d) the x position is kept constant, which is 0.5 but different y value where $y = 0.35$ and $y = 0.65$ respectively. The figure shows that the streamlines appear according to the position of solid cylinder. However, we can see that the streamlines also appear at the top of the enclosure for all position of solid cylinder due to the movement of the top lid wall. In addition, there is no streamline protrude in the solid cylinder. Likewise in isotherm, where we can see that the isotherm lines appear in enclosure in wavy shape. However, the intensity of isotherm is less at the top right of the enclosure for all position of solid cylinder. This maybe due to the various temperature distribution and movement of the top lid wall from left to right. For isentropic, figure depicts the isentropic lines with high intensity at the top of the enclosure for all position of solid cylinder. We also can see that the isentropic lines appear around the solid cylinder, and high density when the solid cylinder is at the bottom of the enclosure as in Figure 16 (d).

The various positions of solid cylinder on the local Nusselt number interfaces with X and local entropy generation at the outer solid cylinder surface is depicted in Figure 17. The local Nusselt number is minimum at the vertical of the cavity wall and maximum between $X = 0.2$ and $X = 0.6$ based on the position of the solid cylinder. The best thermal performance is obtained when the position of the solid cylinder is at the center of the enclosure. In addition, the local entropy generation at the outer solid cylinder is
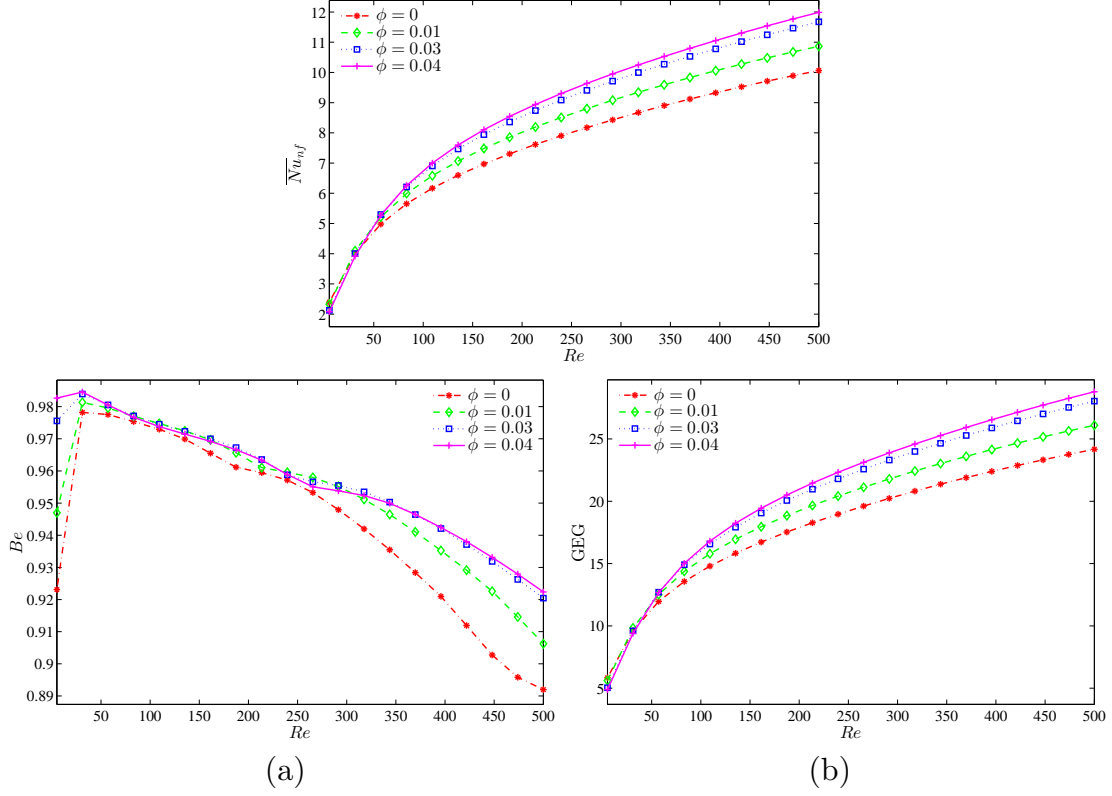
18

Figure 12: Variation of (a) average Nusselt number ($\overline{Nu}_{nf}$), (b) Bejan number (Be) and (c) the global entropy generation (GEG) with Re for different values of ϕ at $Ri = 1$, $R = 0.15$ and $D1$.

in sinusoidal shape. As we can see the local entropy generation is high when the position of the solid cylinder is at the bottom of the enclosure.

Figure 18 illustrates the average Nusselt number, Bejan number and the global entropy generation with nanoparticle volume fraction for different positions of solid cylinder at $Ri = 1$, $Re = 1$, and $R = 0.15$. Different solid cylinder will affect the average Nusselt number, average entropy generation and global entropy generation. We can see that the average Nusselt number and global entropy generation are high when the position of the solid cylinder is at the center of the enclosure. However, both average Nusselt number and the global entropy generation slightly increase as the nanoparticle volume fraction increased for all positions except when the solid is located at the left of the enclosure. The graph in 18 (b) shows that the system is HTI dominant for all positions of solid cylinder since the value of Be is greater than 0.5. As nanoparticle volume fraction number increases, we can see that the Bejan number slightly increased for all position of solid cylinder except when the solid cylinder is located at the right of the enclosure.

5   Conclusions

In this numerical work, the finite difference method is used to analyse the entropy generation and mixed convection in a trapezoidal cavity having differently located solid cylinder filled with Al_2O_3-water nanofluid. The detailed computational results for the streamlines, isotherms and the local entropy generation for different values of the Ra, Re,
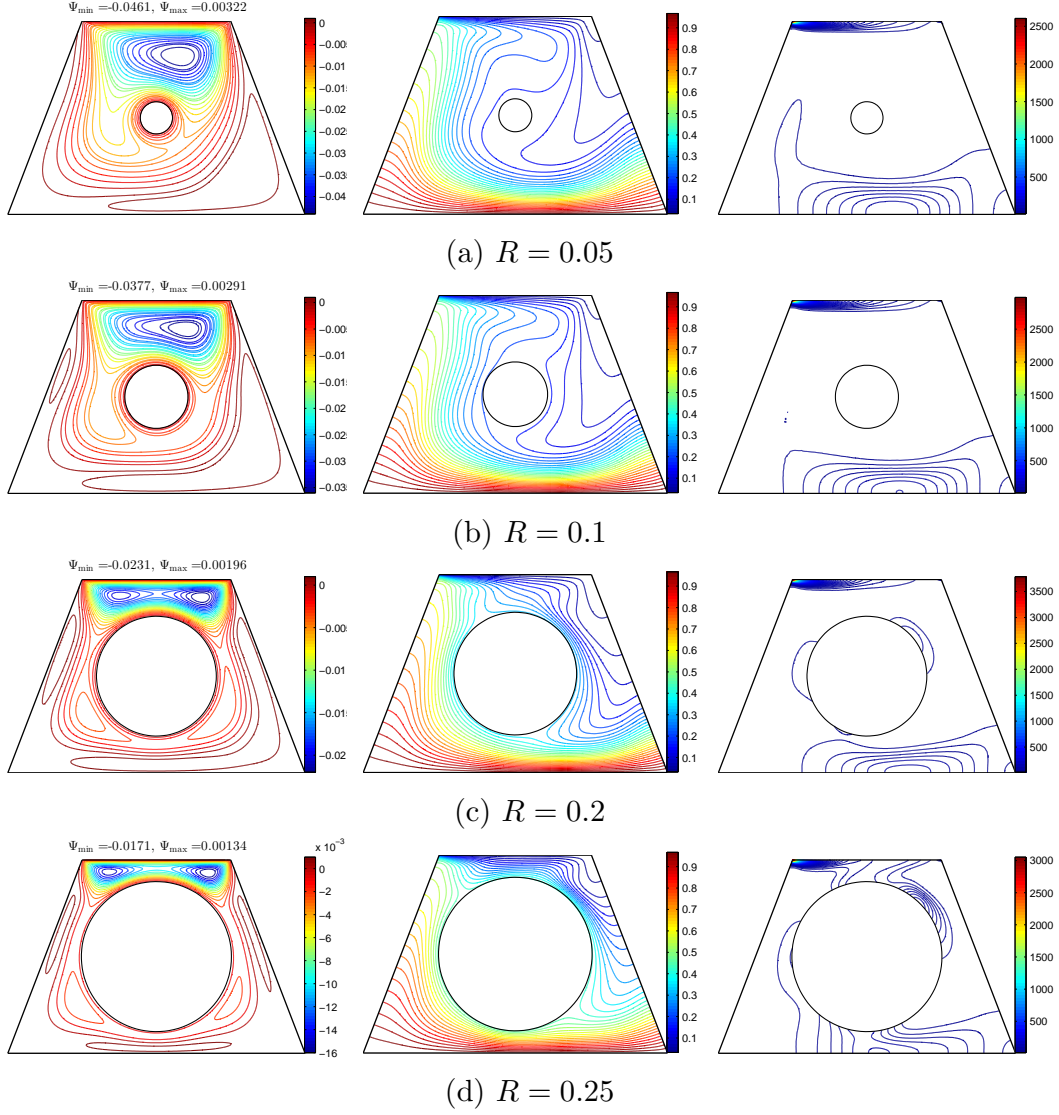
Figure 13: Variation of the streamlines (left), isotherms (middle), and isentropic (right) evolution by solid cylinder radius (R) for $Ri = 1$, $Re = 100$, $\phi = 0.02$ and $D1$.

nanoparticles volume fraction, radius and location of the solid cylinder. Some important conclusions from the study are given below.

1. The different position of solid cylinder tends to influence the flow behaviour in which the temperature distribution and the local entropy generation.

2. Increasing the Richardson number and Reynolds number increases the rate of heat transfer rate as well as a high nanoparticles volume fraction because of increment of buoyancy and viscous forces.

3. The GEG increases with the augmentation of the Ri and Re, while a counteractive behaviour is observed on the average Be. As the Re and Ri increase, the Be number tends to reduce.

4. The Bejan number is decreasing function of the solid cylinder radius for the case of intensive convection regime (Re), while the GEG is an increasing function of the
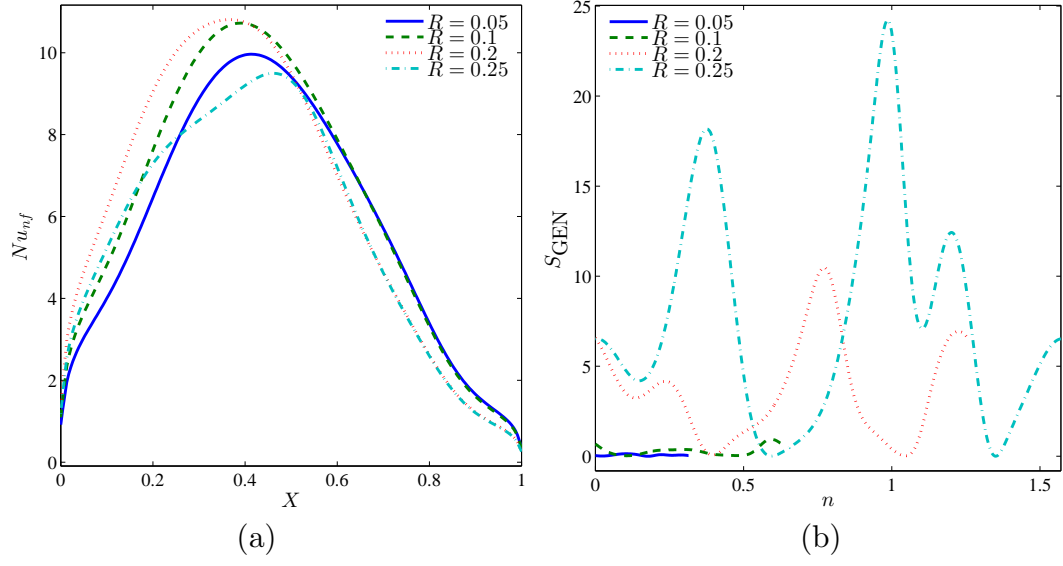
20

Figure 14: Variation of (a) local Nusselt number interfaces with X and (b) local entropy generation at the outer solid cylinder surface for different R at $Ri = 1$, $Re = 100$, $\phi = 0.02$ and $D1$.
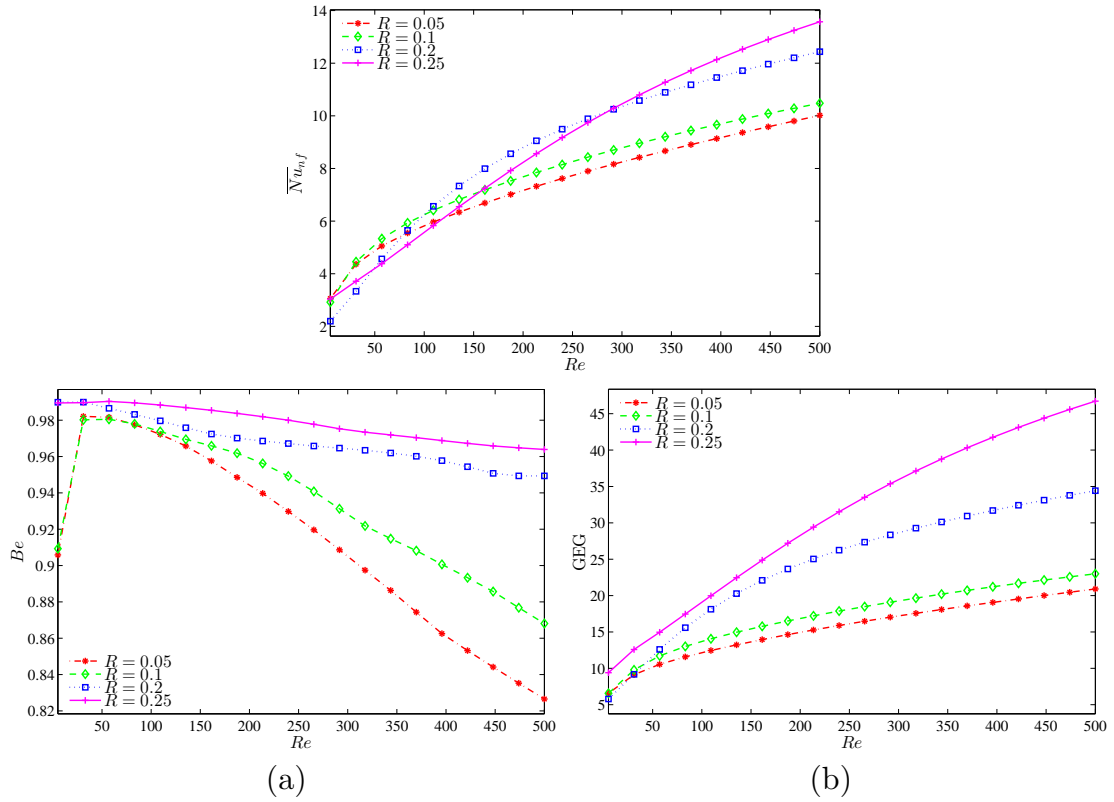

Figure 15: Variation of (a) average Nusselt number ($\overline{Nu}_{nf}$), (b) Bejan number (Be) and (c) the global entropy generation (GEG) with Re for different values of R at $Ri = 1$, $\phi = 0.02$ and $D1$.

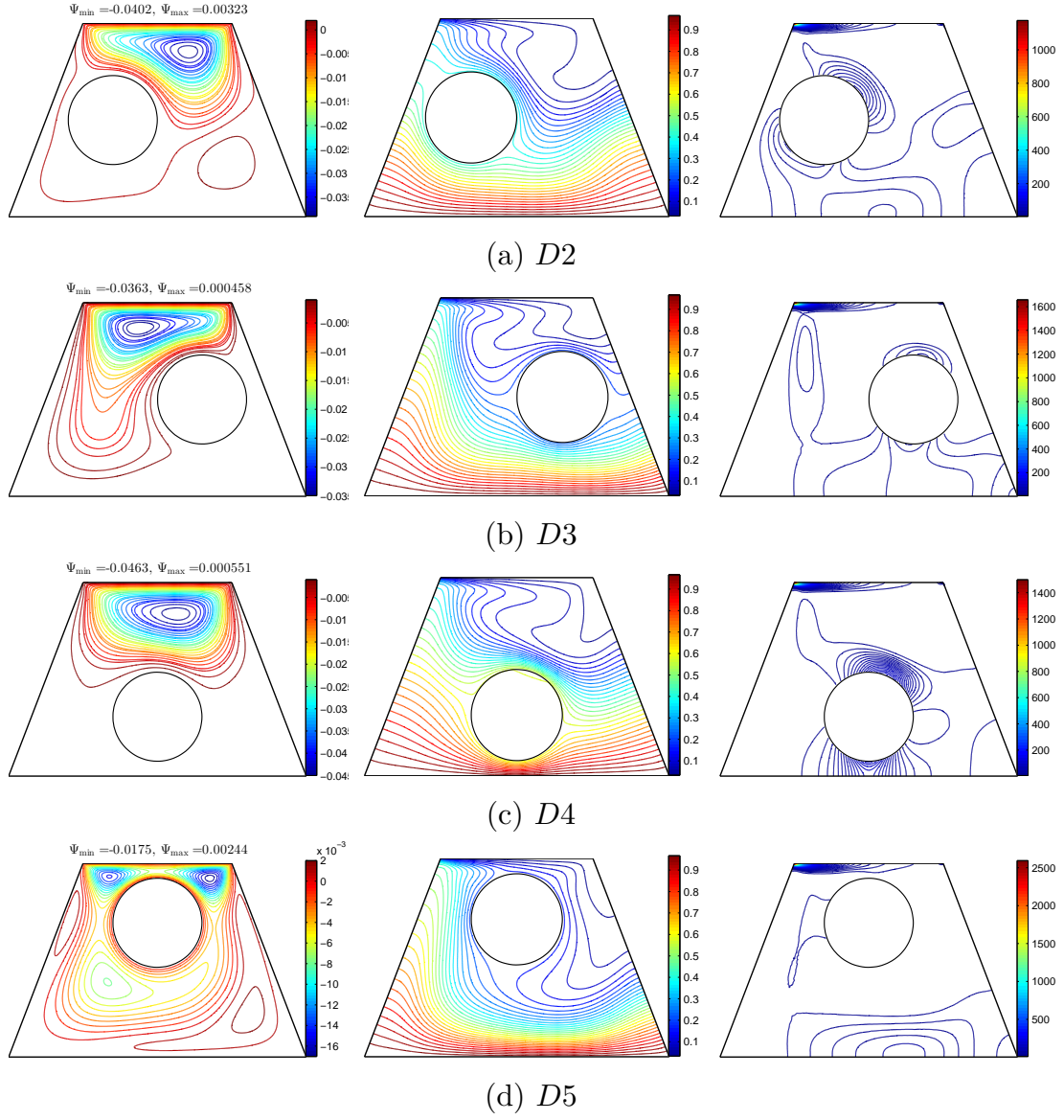size of the solid cylinder radius of the same regime.

Figure 16: Variation of the streamlines (left), isotherms (middle), and isentropic (right) evolution by location of solid cylinder (D) for $Ri = 1$, $Re = 100$, $\phi = 0.02$ and $R = 0.15$.

5. The heat transfer rate and GEG are strong when the solid cylinder located at the centre of the cavity while Bejan number is strong when the solid cylinder located at the top in the cavity.
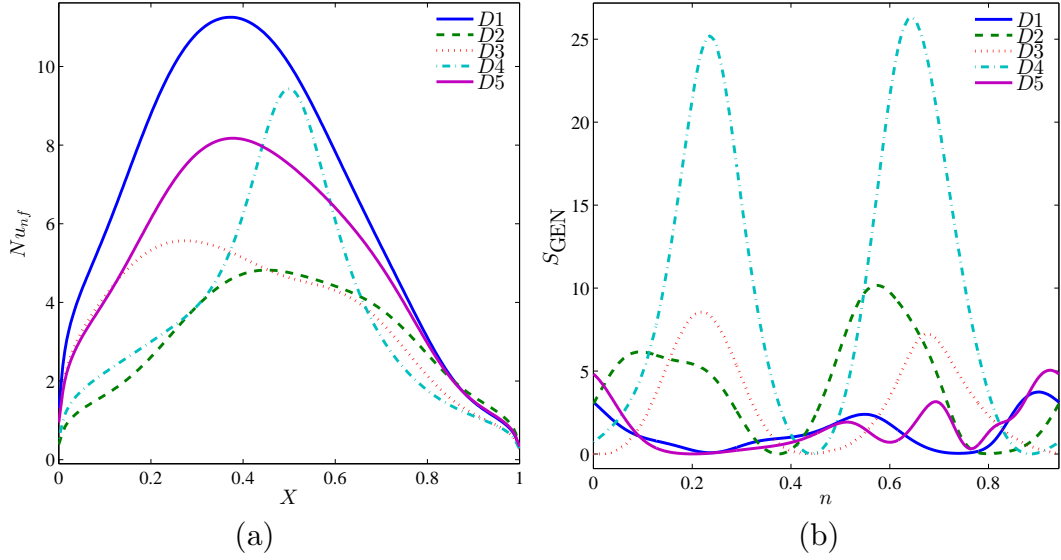
Acknowledgments

Figure 17: Variation of (a) local Nusselt number interfaces with X and (b) local entropy generation at the outer solid cylinder surface for different D at $Ri = 1$, $Re = 100$, $\phi = 0.02$ and $R = 0.15$.
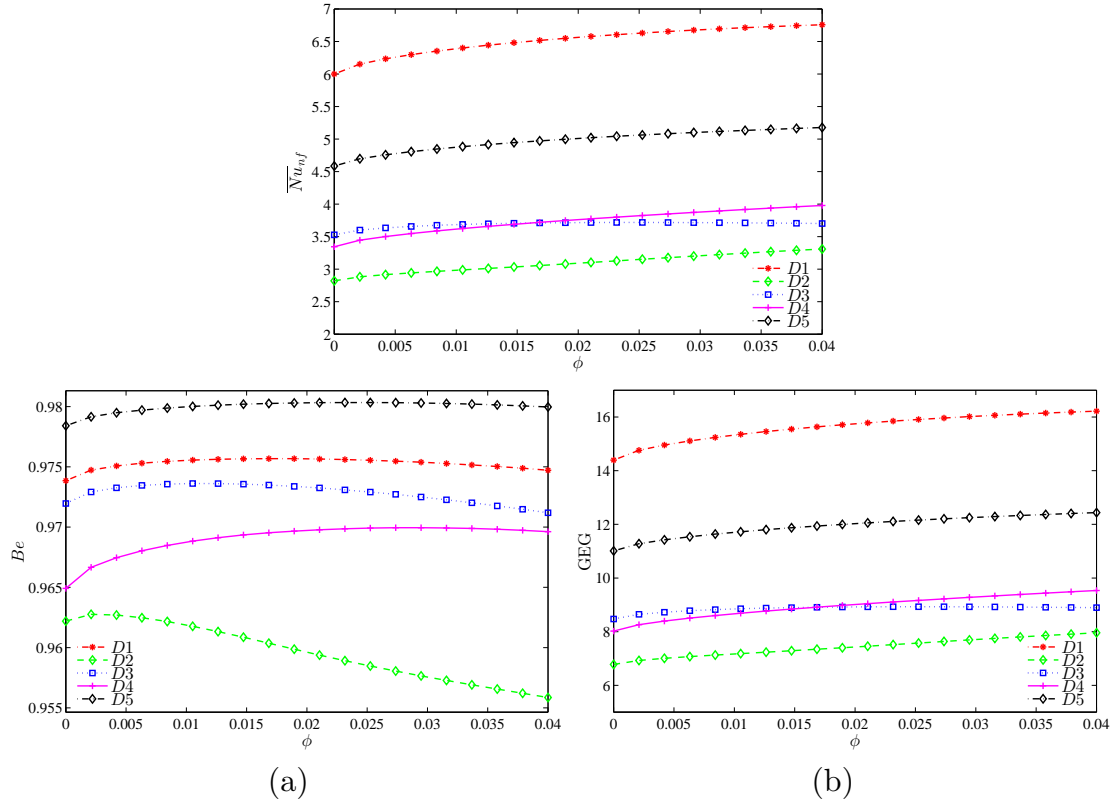

Figure 18: Variation of (a) average Nusselt number ($\overline{Nu}_{nf}$), (b) Bejan number (Be) and (c) the global entropy generation (GEG) with ϕ for different values of D at $Ri = 1$, $Re = 1$ and $R = 0.15$.

References

[1] Roy, M., Basak, T., Roy, S., Pop, I.. Analysis of entropy generation for mixed convection in a square cavity for various thermal boundary

conditions. Numerical Heat Transfer, Part A: Applications 2015;68(1):44–74. doi:10.1080/10407782.2014.955352.

[2] Abbasian Arani, A., Mazrouei Sebdani, S., Mahmoodi, M., Ardeshiri, A., Aliakbari, M.. Numerical study of mixed convection flow in a lid-driven cavity with sinusoidal heating on sidewalls using nanofluid. Superlattices and Microstructures 2012;51:893 – 911.

[3] Khorasanizadeh, H., Nikfar, M., Amanip, J.. Entropy generation of cuwater nanofluid mixed convection in a cavity. European Journal of Mechanics - B/Fluids 2013;37:143 – 152.

[4] Sebdani, S.M., Mahmoodi, M., Hashemi, S.M.. Effect of nanofluid variable properties on mixed convection in a square cavity. International Journal of Thermal Sciences 2012;52:112 – 126.

[5] Nayak, R., Bhattacharyya, S., Pop, I.. Numerical study on mixed convection and entropy generation of a nanofluid in a lid-driven square enclosure. Journal of Heat Transfer 2016;138.

[6] Sivasankaran, S., Sivakumar, V., Prakash, P.. Numerical study on mixed convection in a lid-driven cavity with non-uniform heating on both sidewalls. International Journal of Heat and Mass Transfer 2010;53:4304 – 4315.

[7] Arefmanesh, A., Aghaei, A., Ehteram, H.. Mixed convection heat transfer in a cuowater filled trapezoidal enclosure, effects of various constant and variable properties of the nanofluid. Applied Mathematical Modelling 2016;40:815–831.

[8] Bhattacharya, M., Basak, T., Oztop, H.F., Varol, Y.. Mixed convection and role of multiple solutions in lid-driven trapezoidal enclosures. International Journal of Heat and Mass Transfer 2013;63:366 – 388.

[9] Tmartnhad, I., El Alami, M., Najam, M., Oubarra, A.. Numerical investigation on mixed convection flow in a trapezoidal cavity heated from below. Energy Conversion and Management 2008;49(11):3205 – 3210.

[10] Kareem, A.K., Mohammed, H., Hussein, A.K., Gao, S.. Numerical investigation of mixed convection heat transfer of nanofluids in a lid-driven trapezoidal cavity ????;.

[11] Selimefendigil, F., ztop, H.F.. Modeling and optimization of mhd mixed convection in a lid-driven trapezoidal cavity filled with aluminawater nanofluid: Effects of electrical conductivity models. International Journal of Mechanical Sciences 2018;136:264 – 278.

[12] Aghaei, A., Khorasanizadeh, H., Sheikhzadeh, G., Abbaszadeh, M.. Numerical study of magnetic field on mixed convection and entropy generation of nanofluid in a trapezoidal enclosure. Journal of Magnetism and Magnetic Materials 2016;403:133 – 145.

[13] Abdullah A. A. A. Al-Rashed Ghanbar Ali Sheikhzadeh, A.A.F.M.A.S..M.A.. Effect of a porous medium on flow and mixed convection heat transfer of nanofluids with variable properties in a trapezoidal enclosure. Journal of Thermal Analysis and Calorimetry 2020;139:741 – 754.

[14] Hasib, M.H., Hossen, M.S., Saha, S.. Effect of tilt angle on pure mixed convection flow in trapezoidal cavities filled with water-al2o3 nanofluid. Procedia Engineering 2015;105:388 – 397.

[15] Chamkha, A., Ismael, M.. Magnetic field effect on mixed convection in lid-driven trapezoidal cavities filled with a cuwater nanofluid with an aiding or opposing side wall. Journal of Thermal Science and Engineering Applications 2016;8.

[16] T. Javed Z. Mehmood, I.P.. Mhd-mixed convection flow in a lid-driven trapezoidal cavity under uniformly/non-uniformly heated bottom wall. International Journal of Numerical Methods for Heat & Fluid 2017;27:1231–1248.

[17] Mamun, M., Tanim, T., Rahman, M., Rahman, S., Nagata, S.. Mixed convection analysis in trapezoidal cavity with a moving lid. International Journal of Mechanical and Materials Engineering 2010;5:18–28.

[18] Ababaei, A., Abbaszadeh, M., Chamkha, A., Arefmanesh, A.. Numerical simulation of double diffusive mixed convection and entropy generation in a lid driven trapezoidal enclosure with a heat source. Numerical Heat Transfer Applications 2018;.

[19] Gibanov, N.S., Sheremet, M.A., Oztop, H.F., Abu-Hamdeh, N.. Mixed convection with entropy generation of nanofluid in a lid-driven cavity under the effects of a heat-conducting solid wall and vertical temperature gradient. European Journal of Mechanics - B/Fluids 2018;70:148 – 159.

[20] Astanina, M.S., Sheremet, M.A., Oztop, H.F., Abu-Hamdeh, N.. Mixed convection of al2o3-water nanofluid in a lid-driven cavity having two porous layers. International Journal of Heat and Mass Transfer 2018;118:527 – 537.

[21] Abu-Nada, E., Chamkha, A.J.. Mixed convection flow in a lid-driven inclined square enclosure filled with a nanofluid. European Journal of Mechanics - B/Fluids 2010;29:472 – 482.

[22] Mehmood, K., Hussain, S., Sagheer, M.. Mixed convection in alumina-water nanofluid filled lid-driven square cavity with an isothermally heated square blockage inside with magnetic field effect: Introduction. International Journal of Heat and Mass Transfer 2017;109:397 – 409.

[23] Goodarzi, M., Safaei, M., Vafai, K., Ahmadi, G., Dahari, M., Kazi, S., et al. Investigation of nanofluid mixed convection in a shallow cavity using a two-phase mixture model. International Journal of Thermal Sciences 2014;75:204 – 220.

[24] Chamkha, A.J., Abu-Nada, E.. Mixed convection flow in single- and double-lid driven square cavities filled with wateral2o3 nanofluid: Effect of viscosity models. European Journal of Mechanics - B/Fluids 2012;36:82 – 96.

[25] Akbarinia, A., Behzadmehr, A.. Numerical study of laminar mixed convection of a nanofluid in horizontal curved tubes. Applied Thermal Engineering 2007;8:1327 – 1337.

[26] Alinia, M., Ganji, D., Gorji-Bandpy, M.. Numerical study of mixed convection in an inclined two sided lid driven cavity filled with nanofluid using two-phase mixture model. International Communications in Heat and Mass Transfer 2011;38:1428 – 1435.

[27] Shariat, M., Akbarinia, A., Nezhad, A.H., Behzadmehr, A., Laur, R.. Numerical study of two phase laminar mixed convection nanofluid in elliptic ducts. Applied Thermal Engineering 2011;31:2348 – 2359.

[28] Alsabery, A., Ishak, S., Chamkha, A., Hashim, I.. Entropy generation analysis and natural convection in a nanofluid-filled square cavity with a concentric solid insert and different temperature distributions. Entropy 2018;20:336. doi:10.3390/e20050336.

[29] Alsabery, A., Siddheshwar, P., Saleh, H., Hashim, I.. Transient free convective heat transfer in nanoliquid-saturated porous square cavity with a concentric solid insert and sinusoidal boundary condition. Superlattices and Microstructures 2016;100:1006 – 1028.

[30] Mahmoodi, M., Sebdani, S.M.. Natural convection in a square cavity containing a nanofluid and an adiabatic square block at the center. Superlattices and Microstructures 2012;52(2):261 – 275.

[31] Sheremet, M., ztop, H., Pop, I., Abu-Hamdeh, N.. Analysis of entropy generation in natural convection of nanofluid inside a square cavity having hot solid block: Tiwari and das model. Entropy 2015;18:9. doi:10.3390/e18010009.

[32] Alnajem, M.H.S., Alsabery, A.I., Hashim, I.. Entropy generation and natural convection in a wavy-wall cavity filled with a nanofluid and containing an inner solid cylinder. IOP Conference Series: Materials Science and Engineering 2019;518:032044.

[33] Alsabery, A., Sheremet, M., Chamkha, A., Hashim, I.. Impact of nonhomogeneous nanofluid model on transient mixed convection in a double lid-driven wavy cavity involving solid circular cylinder. International Journal of Mechanical Sciences 2019;150:637 – 655.

[34] Selimefendigil, F., ztop, H.F., Chamkha, A.J.. Analysis of mixed convection of nanofluid in a 3d lid-driven trapezoidal cavity with flexible side surfaces and inner cylinder. International Communications in Heat and Mass Transfer 2017;87:40 – 51.

[35] Liao, C.C., Lin, C.A.. Mixed convection of a heated rotating cylinder in a square enclosure. International Journal of Heat and Mass Transfer 2014;72:9 – 22.

[36] Alsabery, A., Ismael, M., Chamkha, A., Hashim, I.. Numerical investigation of mixed convection and entropy generation in a wavy-walled cavity filled with nanofluid and involving a rotating cylinder. Entropy 2018;20:664. doi:10.3390/e20090664.

[37] Rahman, M.M., Alim, M., Mamun, M.A.H.. Finite element analysis of mixed convection in a rectangular cavity with a heat-conducting horizontal circular cylinder. Nonlinear Analysis: Modelling and Control 2009;14:217 – 247.

[38] Rahman, M.M., Alim, M.. Mhd mixed convection flow in a vertical lid-driven square enclosure including a heat conducting horizontal circular cylinder with joule heating. Nonlinear Analysis: Modelling and Control 2010;15:199 – 211.

[39] Shariat, M., Akbarinia, A., Nezhad, A.H., Behzadmehr, A., Laur, R.. Mhd mixed convection of nanofluid filled partially heated triangular enclosure with a rotating adiabatic cylinder. Journal of the Taiwan Institute of Chemical Engineers 2014;45:2150 – 2162.

[40] Rahman, M., Alim, M.A., Saha, S., Chowdhury, M.. Mixed convection in a vented square cavity with a heat conducting horizontal solid circular cylinder. Journal of Naval Architecture and Marine Engineering 2008;5:37–46. doi:10.3329/jname.v5i2.2504.

[41] Chatterjee, D., Gupta, S.K., Mondal, B.. Mixed convective transport in a lid-driven cavity containing a nanofluid and a rotating circular cylinder at the center. International Communications in Heat and Mass Transfer 2014;56:71 – 78.

[42] Billah, M., Rahman, M., Sharif, U.M., Rahim, N., Saidur, R., Hasanuzzaman, M.. Numerical analysis of fluid flow due to mixed convection in a lid-driven cavity having a heated circular hollow cylinder. International Communications in Heat and Mass Transfer 2011;38:1093 – 1103.

[43] Gangawane, K.M., Oztop, H.F., Abu-Hamdeh, N.. Mixed convection characteristic in a lid-driven cavity containing heated triangular block: Effect of location and size of block. International Journal of Heat and Mass Transfer 2018;124:860 – 875.

[44] Hussain, S.H., Hussein, A.K.. Mixed convection heat transfer in a differentially heated square enclosure with a conductive rotating circular cylinder at different vertical locations. International Communications in Heat and Mass Transfer 2011;38:263 – 274.

[45] Alsabery, A.I., Ismael, M.A., Chamkha, A.J., Hashim, I.. Mixed convection of al2o3-water nanofluid in a double lid-driven square cavity with a solid inner insert using buongiornos two-phase model. International Journal of Heat and Mass Transfer 2018;119:939 – 961.

[46] Corcione, M.. Empirical correlating equations for predicting the effective thermal conductivity and dynamic viscosity of nanofluids. Energy Conversion and Management 2011;52(1):789–793.

[47] Ilis, G.G., Mobedi, M., Sunden, B.. Effect of aspect ratio on entropy generation in a rectangular cavity with differentially heated vertical walls. International Communications in Heat and Mass Transfer 2008;35(6):696–703.

[48] Alsabery, A.I., Tayebi, T., Chamkha, A.J., Hashim, I.. Effect of rotating solid cylinder on entropy generation and convective heat transfer in a wavy porous cavity heated from below. International Communications in Heat and Mass Transfer 2018;95:197–209.

[49] Khanafer, K., Aithal, S.M.. Laminar mixed convection flow and heat transfer characteristics in a lid driven cavity with a circular cylinder. International Journal of Heat and Mass Transfer 2013;66:200–209.

[50] Corcione, M., Cianfrini, M., Quintino, A.. Two-phase mixture modeling of natural convection of nanofluids with temperature-dependent properties. International Journal of Thermal Sciences 2013;71:182–195.

[51] Chon, C.H., Kihm, K.D., Lee, S.P., Choi, S.U.. Empirical correlation finding the role of temperature and particle size for nanofluid (al2o3) thermal conductivity enhancement. Applied Physics Letters 2005;87(15):3107.

[52] Ho, C., Liu, W., Chang, Y., Lin, C.. Natural convection heat transfer of alumina-water nanofluid in vertical square enclosures: An experimental study. International Journal of Thermal Sciences 2010;49(8):1345–1353.

[53] Bergman, T.L., Incropera, F.P.. Introduction to heat transfer, 6$^{\text{th}}$ edition. New York: Wiley; 2011.